In Vivo SILAC-Based Proteomics Reveals Phosphoproteome Changes during Mouse Skin Carcinogenesis

Sara Zanivan,[1,3,*] Alexander Meves,[2,4] Kristina Behrendt,[6] Erwin M. Schoof,[7] Lisa J. Neilson,[3] Jürgen Cox,[1] Hao R. Tang,[3] Gabriela Kalna,[3] Janine H. van Ree,[5] Jan M. van Deursen,[5] Carol S. Trempus,[8] Laura M. Machesky,[3] Rune Linding,[7] Sara A. Wickström,[6] Reinhard Fässler,[2] and Matthias Mann[1,9,*]
[1]Department of Proteomics and Signal Transduction
[2]Department of Molecular Medicine
Max-Planck Institute of Biochemistry, Am Klopferspitz 18, 82152 Martinsried, Germany
[3]Beatson Institute for Cancer Research, Garscube Estate, Switchback Road, Bearsden, Glasgow G61 1BD, UK
[4]Department of Dermatology
[5]Department of Pediatric and Adolescent Medicine
Mayo Clinic College of Medicine, Rochester, MN 55905, USA
[6]Paul Gerson Unna Group "Skin Homeostasis and Ageing," Max-Planck Institute for Biology of Ageing, Gleueler Str. 50a, 50931 Köln, Germany
[7]Cellular Signal Integration Group (C-SIG), Center for Biological Sequence Analysis (CBS), Department of Systems Biology, Technical University of Denmark (DTU), DK-2800 Lyngby, Denmark
[8]Matrix Biology Group, Laboratory of Respiratory Biology National Institute of Environmental Health Sciences Research Triangle Park, NC 27709, USA
[9]The Novo Nordisk Foundation Center for Protein Research, Faculty of Health Sciences, University of Copenhagen, 2200 Copenhagen, Denmark
*Correspondence: s.zanivan@beatson.gla.ac.uk (S.Z.), mmann@biochem.mpg.de (M.M.)
http://dx.doi.org/10.1016/j.celrep.2013.01.003

SUMMARY

Cancer progresses through distinct stages, and mouse models recapitulating traits of this progression are frequently used to explore genetic, morphological, and pharmacological aspects of tumor development. To complement genomic investigations of this process, we here quantify phosphoproteomic changes in skin cancer development using the SILAC mouse technology coupled to high-resolution mass spectrometry. We distill protein expression signatures from our data that distinguish between skin cancer stages. A distinct phosphoproteome of the two stages of cancer progression is identified that correlates with perturbed cell growth and implicates cell adhesion as a major driver of malignancy. Importantly, integrated analysis of phosphoproteomic data and prediction of kinase activity revealed PAK4-PKC/SRC network to be highly deregulated in SCC but not in papilloma. This detailed molecular picture, both at the proteome and phosphoproteome level, will prove useful for the study of mechanisms of tumor progression.

INTRODUCTION

Mouse models of cancer are a resource of great potential in cancer research and they have provided important insights into tumor biology (Marcotte and Muller, 2008; Walrath et al., 2010). They have helped in confirming gene function, identifying tumor markers, and contributing to a better understanding of the cellular and molecular mechanisms of tumor initiation and the multistage processes of tumorigenesis. In addition to detailed functional studies, these models have been investigated with large-scale and unbiased "omics" technologies—usually in the form of measuring gene expression changes with microarrays (Hummerich et al., 2006; Landis et al., 2005). However, messenger RNA (mRNA) levels do not correlate well with protein levels (Tian et al., 2004) or provide information on protein activity. Therefore, more advanced large-scale analyses of proteins and their posttranslational modifications (PTMs) are needed to understand the complex processes involved in cancer development. While this has been a central aim of the proteomics community, daunting technological challenges have so far prevented proteomics from complementing the ubiquitous genomic technologies at a similar level of comprehensiveness (Hanash and Taguchi, 2010; Harsha and Pandey, 2010; Pawson and Scott, 2005).

Cancer is intimately associated with somatic alterations (Stratton et al., 2009). Mutations that initiate the tumor process often occur in protein kinase pathways. A prominent example is a single base mutation of HRas, which strongly impinges on the Mapk pathways, or the kinase BRaf, which are associated with a large fraction of epithelial tumors (Davies et al., 2002; Reddy et al., 1982). Such mutations have direct effects on the activity of specific signaling pathways, which can in principle be detected by large-scale analysis of the phosphorylation status of proteins in tumors ("phosphoproteomics"). Alterations

in signaling pathways drive cellular changes, including changes in gene expression, ultimately resulting in altered protein levels, which can be measured by quantitative proteomics. Therefore, proteomics can complement genomic studies that are well suited to determine alterations in the cancer genome and gene expression levels.

A well-established system to study tumor progression in mice is the chemical induced multistage skin carcinogenesis model (Abel et al., 2009). Beyond the generic advantages of mouse models, such as reduced genetic variability, this model offers three distinct stages for proteomic investigation, representing precancerous, benign and malignant tumors. Here, we use an advanced proteomic workflow employing high-resolution mass spectrometry (MS) in combination with stable isotope labeling by amino acids in cell culture (SILAC) (Mann, 2006; Ong et al., 2002) to quantify the proteome and the phosphoproteome of tumor tissues. For phosphoproteomics, we employed an established enrichment protocol, which has been used successfully with SILAC to analyze cell signaling (Olsen et al., 2006). However, it is still challenging to perform quantitative proteomics studies in vivo and, to our knowledge, there are to date no quantitative in-depth studies of the phosphoproteome in vivo in cancer. We have previously set the stage for such studies by establishing SILAC labeled mice as a powerful tool to perform in vivo quantitative proteomic studies of organs, tissues, and cells (Krüger et al., 2008; Ostasiewicz et al., 2010). Additionally, we and others have shown that phosphorylations can be studied in vivo (Monetti et al., 2011; Rikova et al., 2007; Villén et al., 2007; Zanivan et al., 2008).

In the present paper, we combined the SILAC mouse technology in a "spike-in" fashion (Geiger et al., 2011) with a chemical-induced carcinogenesis tumor model. A single treatment of the skin with the carcinogen DMBA initiates skin carcinogenesis by inducing an activating mutation of HRas. Further repeated applications of the tumor promoter 12-O-tetradecanoylphorbol-13-acetate (TPA) provoke the development of a premalignant lesion, papilloma (Pap). Papilloma mirrors human actinic keratosis (AK) and can progress to the malignant tumor, squamous cell carcinoma (SCC) (Roberts et al., 2007). We accurately identified and quantified a considerable part of the proteome and phosphoproteome of TPA-treated skin (referred to as TPA), Pap, and SCC. With this approach, we provide evidence that distinct parts of the proteome and phosphoproteome are regulated during the different steps of carcinogenesis and identify specific processes that become deregulated. Illustrating the relevance of this approach to human tumors, we validated altered expression levels of specific candidates for cancer progression in human tumor tissues and confirmed their invasive potential.

RESULTS

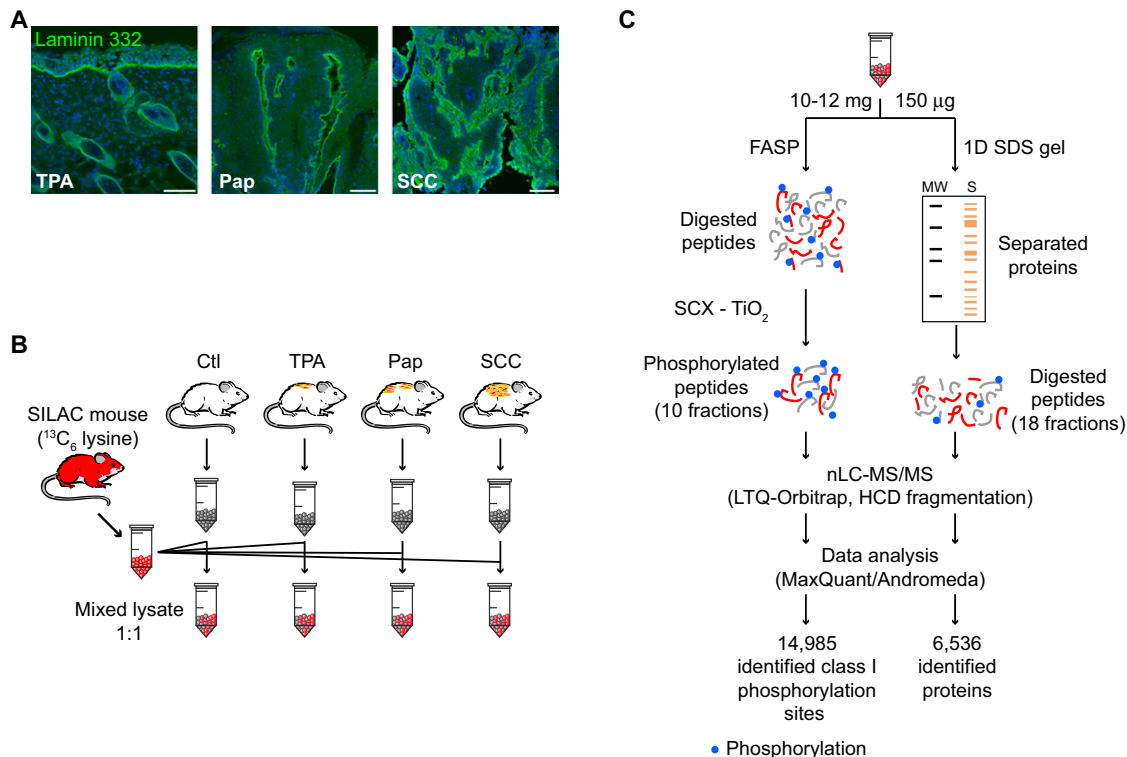### SILAC Mouse Model to Quantify Phosphoproteome in Cancer Progression

We isolated tissue samples from four defined stages of mouse skin cancer development: (1) non-TPA-treated control skin (Ctl), (2) TPA-treated skin, (3) lesions that have progressed to the papilloma stage and finally to the (4) carcinoma stage.

Tumors were classified as Pap or SCC according to histological analysis and further validated by laminin 332 staining performed on tissue. As expected, the basement membrane (BM) was well organized in TPA and Pap, but not in the SCC where the BM accumulated at the interface between stroma and invading tumor cells (Figure 1A).

The skin is an elastic tissue rich in collagens and keratins, making in-depth proteomic analysis very difficult with standard MS protocols. Indeed, use of lysis buffers containing urea, which is compatible with MS, resulted in low yields of extracted proteins and incomplete protease cleavage. Therefore we used a lysis buffer containing 4% SDS. We separated the proteome by 1D SDS-PAGE followed by in-gel digestion. For the phosphoproteome, we also solubilized proteins in SDS, but digested them on filter (Wisniewski et al., 2009), fractionated by strong cation exchange chromatography (SCX) and subsequently enriched for phosphorylated peptides using titanium dioxide (TiO$_2$) (Larsen et al., 2005). Peptides were then analyzed with high-resolution liquid chromatography-tandem mass spectrometry (nLC MS/MS) on a hybrid linear ion trap Orbitrap instrument. To accurately assign to each protein the expression and phosphorylation level, we used a spike-in SILAC approach (Geiger et al., 2011). For this, a labeled proteome standard with a protein composition and abundance as similar as possible to the skin tissue samples to be analyzed was required, and we tested the suitability of the skin from SILAC mice. We mixed an equal amount of the SILAC standard lysate to each tissue lysate at a ratio of 1:1 and processed the samples for MS analysis (Figures 1B and 1C). A comparable number of proteins and phosphorylation sites were quantified in all the analyzed samples (Figures S1A and S1B). Additionally, on average, more than 95% of the quantified proteins and phosphorylation sites in the skin, Ctl or TPA, were within a 4-fold ratio compared to the SILAC skin. In the tumors, the percentage was higher than 90% (Figures S1C and S1D). By ensuring that the large majority of proteins were in an easily quantified range, these results validate the SILAC skin as an excellent spike-in standard for accurate proteome quantification.

From three measurements, which comprised a total of more than 400 MS runs, we identified 6,536 proteins (Table S1) and 14,985 class I phosphorylation sites (sites with high phospholocalization probability for a single amino acid) (Table S2) with a 0.87 and 0.37 ppm average absolute peptide mass error, respectively. Phosphorylation sites were localized with single amino acid resolution (median localization probability 0.999) and comprised 13,173 Ser, 1,708 Thr, and 104 Tyr sites, of which 40% have not been previously reported.

To evaluate the reproducibility of our quantitative approach we measured the correlation of the normalized SILAC ratio for proteins and phosphorylation sites between measurements. While TPA, Pap, and SCC showed high similarity (average R^2 of 0.9 for proteome and 0.8 for phosphoproteome), the correlation was only 0.5 for the control skin (Figures S1E and S1F and Table S3). This low correlation was attributed to the nonreproducible isolation of the samples that occurred in the skin samples alone. Although we included the proteome and phosphoproteome of the control skin as a resource of proteins and phosphorylation sites identified in the mouse skin, we did not consider

Figure 1. SILAC Mouse Skin as Standard for In Vivo Quantitative Phosphoproteomics
(A) Confocal images of frozen sections of TPA, Pap, and SCC stained for laminin 332. Nuclei are stained with DAPI (blue). Images are representative of the staining from three mice. Scale bar, 100 μm.
(B) SILAC-based workflow.
(C) MS analysis workflow. Results represent three to five MS measurements. MW, standard molecular weight; S, mixed lysate.
See also Tables S1, S2, and Figure S1.

those samples any further for our study, and we estimated proteomic changes in tumors by comparison to TPA.

A total of 3,457 proteins and 5,249 phosphorylation sites were accurately quantified and used for further bioinformatic analysis (Tables S4 and S5). This set includes proteins with a large variety of functions. According to gene ontology (GO) annotation reported in the UniProt database, 116 proteins and 59 phosphorylated proteins are involved in cell adhesion, 92 proteins and 85 phosphorylated proteins in protein kinase activity, and 38 proteins and 41 phosphorylated proteins in transcription cofactor activity.
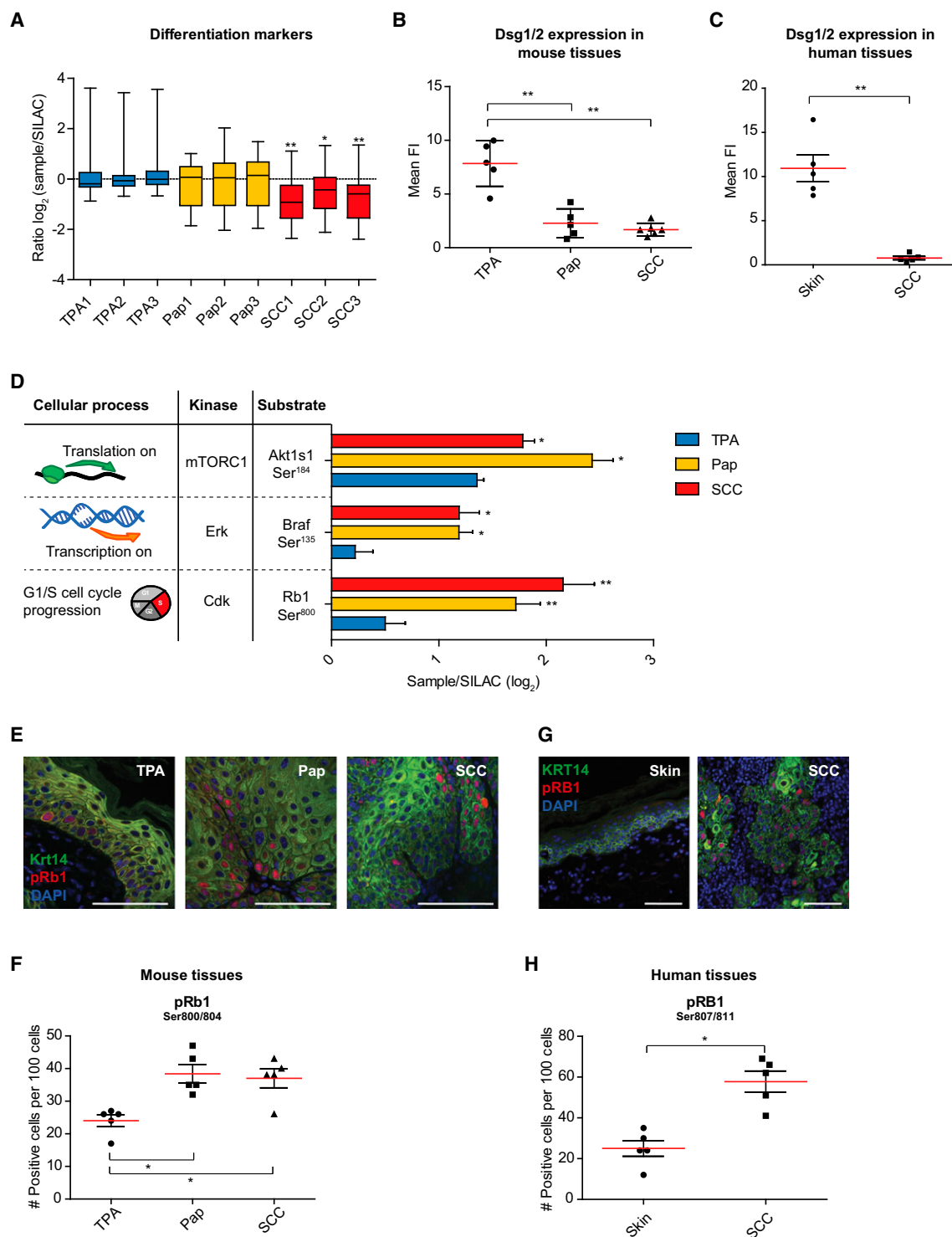
Together, these data show that our screen on TPA-treated skin and tumor tissues was accurate and reproducible and that it quantitatively probed the proteome and phosphoproteome to considerable depths in vivo.

Large-Scale Phosphoproteomics Faithfully Recapitulates Known Molecular Mechanisms in Tumorigenesis

The state of dedifferentiation of a tumor is often used to evaluate its malignancy (Ehrenreiter et al., 2009). As expected, the differentiation markers Krt10 and Krt1 were expressed at substantially lower levels in SCC compared to TPA and Pap (Tables S1 and S4). Additionally the expression levels of 25 proteins involved

in skin differentiation (Table S6) (Meves et al., 2011) were significantly downregulated in SCC (Figure 2A). These included the desmosomal proteins Dsg1 and Dsg2. Immunofluorescence staining of mouse tissues with antibody against Dsg1/2 confirmed the decreased expression of these proteins in SCC (Figures 2B and S2A). Interestingly, we found Dsg1/2 downregulated also in tissues from SCC patients (Figures 2C and S2B), which has been previously observed for SCC of different origin (Wong et al., 2008). Likewise, a number of other proteins that showed altered expression levels are known to be regulated in tumor development (Kurzen et al., 2003), providing a positive control for our screen.

One of the fundamental traits of cancer cells is their sustained growth and proliferation often reflected by the deregulation of cyclin-dependent kinase (CDK), mTOR, and ERK/MAPK pathways (Hanahan and Weinberg, 2011). Such alterations are generally driven by modified phosphorylation levels, of proteins involved in these pathways. Our phosphoproteome data recapitulate these alterations. Notably, the cell cycle regulator Rb1 can be inactivated by phosphorylation at Ser[800] (pRb1) by Cdk (Roesch et al., 2005) and thereby promote mitosis. Rb1 has previously been reported to be highly phosphorylated in SCC of the DMBA-TPA mouse model and in human SCC (Nilsson et al., 2004). Our MS analysis found significantly higher levels

Figure 2. Known Processes in Cancer Development Recapitulated by Quantitative Proteomics In Vivo

(A) Whiskers plot (minimum and maximum value) of normalized SILAC ratio of 25 proteins involved in keratinocytes differentiation (see Table S6). 1–3 indicates the MS measurements. p values were calculated between TPA and SCC of the same set of MS measurement.

(B and C) Quantification of Dsg1/2 immunofluorescence in mouse tissues (B) TPA (n = 5), Pap (n = 5), and SCC (n = 6) and human tissues (C) normal skin (n = 5), SCC (n = 5). n = number of mice/patients. FI, fluorescence intensity.

(D) Normalized SILAC ratios of phosphorylation sites (substrate) involved in processes deregulated in cancer. For each site, the kinase is indicated. Bars = SD (n > 2, n = number of quantifications). p values were calculated between Pap/SCC and TPA.

(legend continued on next page)

of pRb1 in Pap and SCC compared to TPA-treated skin (Figure 2D), which we confirmed by immunofluorescence analysis of tissue sections (Figures 2E and 2F). Importantly, we observed similar results by immunostaining of human skin and SCC tissue samples (Figures 2G and 2H). Phosphorylation of Akt1s1 at Ser[184] (pAkt1s1) indicates mTOR activity (Wang et al., 2008). Here, we found pAkt1ts1 levels to increase significantly in tumors compared to TPA (Figure 2D). Finally, increased phosphorylation levels of BRaf at Ser[135] were measured, pointing to elevated activity of the Erk/Mapk pathway (Ritt et al., 2010) (Figure 2D). These specific examples are only a small fraction of the several thousand sites quantified. Their validity serves as a clear indicator of the relevance of our phosphoproteomic data set.

Phosphoproteomic Alteration in Skin Carcinogenesis

The SILAC ratios of quantified proteins and phosphorylation sites were clustered using correlation distances between averages and this revealed a close similarity between Pap (P) and SCC (S) but striking differences between TPA (T) and tumor. Nevertheless, there was a small but distinct subset of proteins regulated only in SCC (Figures 3A and 3B).

We thus investigated the phosphoproteomic changes during skin carcinogenesis in more detail. By means of ANOVA test corrected for permutation based false discovery rate (FDR), we identified proteins and phosphorylation sites significantly regulated in tumors compared to TPA (Tables S4 and S5). Of the 3,457 quantified proteins, 483 and 332 were upregulated in Pap and SCC, respectively, representing the 10%–14% of the proteome. Furthermore, 660 and 720 proteins were downregulated, representing the 19%–21% of the proteome (Figure 3C). Of the 5,249 phosphorylation sites, 825 and 970 were upregulated in Pap and SCC, respectively, while 720 and 1,017 were downregulated (Figure 3D). This indicated that 14%–16% of the phosphoproteome was upregulated, whereas 18%–19% downregulated. As anticipated by the hierarchical clustering, 5% of the proteins and phosphorylation sites were regulated only in the SCC (Figures 3C and 3D).

When we combined the phosphoproteome and proteome data sets, we found that we could measure the corresponding protein abundance for 45% of the quantified phosphorylation sites (Figure 3E). For half of these sites, protein and phosphorylation levels were regulated accordingly, while for the other half significant regulation occurred only at the level of phosphorylation (Figure 3F). Only 1% of the phosphorylation sites showed opposite regulation at the protein and phosphorylation levels. This subset included the tumor-regulated pyruvate kinase (Pkm2), which was found upregulated at the protein level, but with decreased phosphorylation level of Ser[127].

Altogether these data show that one-third of the proteome and phosphoproteome of the skin and tumor tissues are expressed at different levels, that there are detectable proteomic differences between benign and malignant tumor tissues, and that

a complementary analysis of proteome and phosphoproteome in our study is necessary for a more comprehensive understanding of the molecular mechanisms in carcinogenesis.

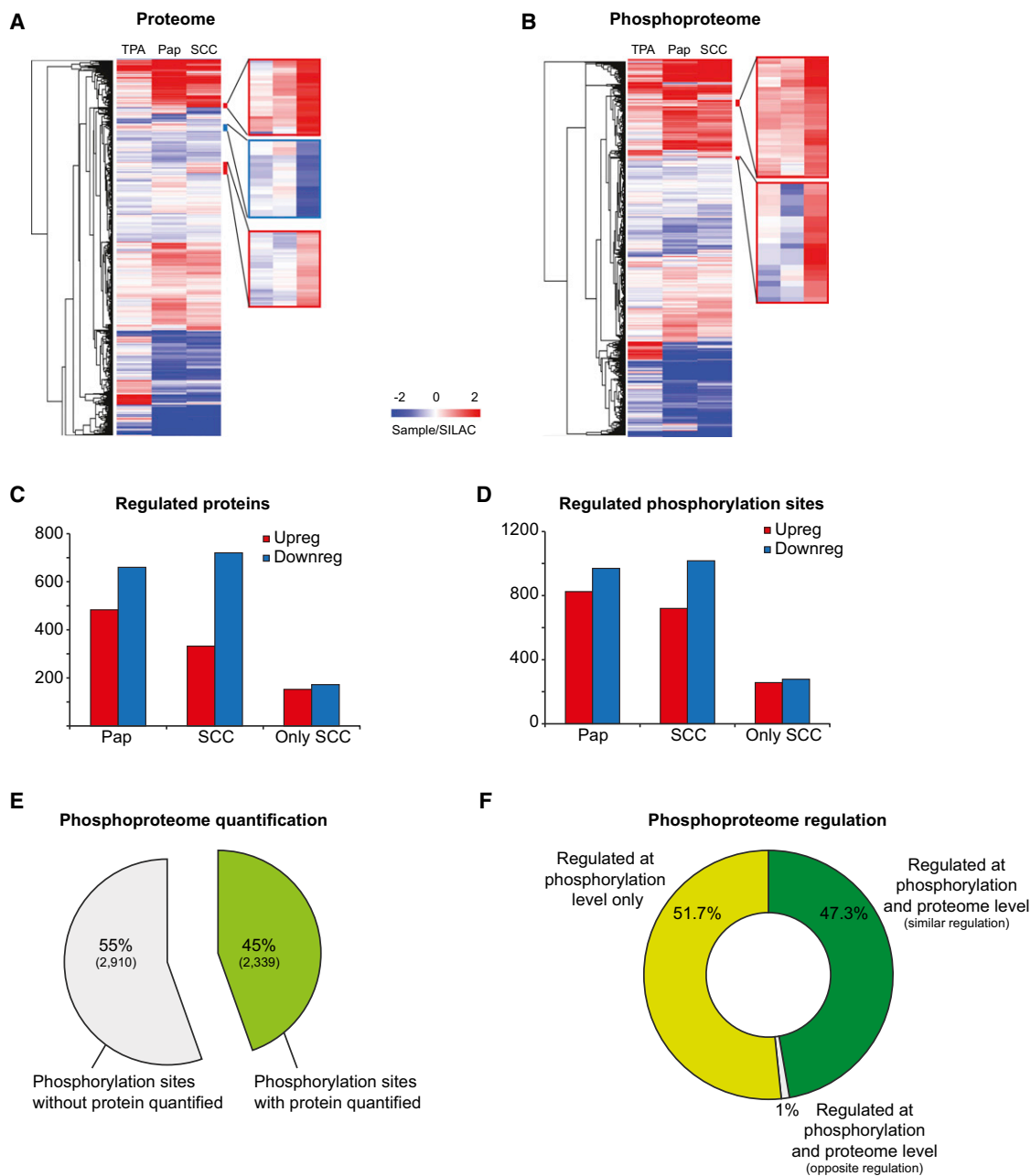### Functional Portrait of Skin Carcinogenesis

To gain insights on the processes regulated in skin cancer progression, we identified the GO categories (Figures 4A and 4B and Table S7) overrepresented in proteins regulated in Pap and SCC compared to TPA. Most of the categories covered major pathways deregulated in cancer such as cell cycle, transcription, translation, apoptosis, cell adhesion, and metabolic process. Additionally, this analysis revealed a prominent fraction of proteins with catalytic, binding, and structural activities. This suggested that functional and physical protein-protein interactions are highly regulated during cancer development and we therefore visualized this information in a systematic way in the STRING environment (Szklarczyk et al., 2011). Since cell adhesion is a prominent process involved in cancer development, and overrepresented in SCC (Figure 4A), we integrated detailed information from the literature (Table S8) into the STRING analysis and visualized the results in Cytoscape. We built up color-coded networks with stage-related information (Figures S3A and S3B). As expected, tightly connected subnetworks emerged, where most of the proteins were already regulated in the Pap stage (Figure 4C). Downregulated subnetworks clearly highlighted altered metabolism. Notably, tumor cells switch their metabolism to anaerobic glycolysis (Ohlrogge et al., 2009). Accordingly, the pyruvate dehydrogenases (Pdha1, Pdhb) reduced expression levels in Pap and SCC compared to TPA. Conversely, Ldha and Pkm2, key enzymes for the synthesis of lactate, increased expression levels (Table S4). Also glutathione, retinol and lipid metabolisms were found downregulated. Interestingly, components of the latter were downregulated specifically in the SCC. Finally, a major subnetwork included cell adhesion proteins. The subnetworks extracted from upregulated proteins and phosphorylation sites revealed a clear difference between benign and malignant tumor and distinct connections between phosphorylation and proteome changes. For example, the cell cycle-related subnetwork involved more phosphorylation than protein expression changes that occurred already in the Pap, while the DNA replication complex Mcm 2-7 was upregulated only in the SCC stage. Also proteins involved in nuclear transport were found regulated at phosphorylation level already in the Pap. Similarly, RNA binding proteins were regulated at the phosphorylation level but formed a cluster with ribosomal subunits, which were regulated at the expression level. In contrast, apoptosis was regulated only at the protein level, likewise for proteins involved in the immune system. As for the downregulated proteins, some changes were found in metabolic pathways, including glutathione and nucleotide metabolism. Finally, cell adhesion proteins formed a predominant subnetwork. Itgβ1, Itgα1, Rac2, Vasp, Src, and fibronectin (Fn1) were identified as cell adhesion hubs with higher number of edges

---

(E and G) Representative immunofluorescence of pRB1 in mouse (E) and human (G) Ker14^{+} cells. Scale bar, 50 μm.

(F and H) Quantification of immunofluorescence of pRB1 in TPA, Pap and SCC mouse (E), and skin and SCC human (G) tissue sections. The quantification is based on the number of positive nuclei per 100 Krt14^{+} cells (y axis). * = p < 0.05 (n = 5).

See also Figure S2.

Figure 3. Proteomic and Phosphoproteomic Differences between Skin and Tumor Tissues

(A and B) Heatmaps and hierarchical clustering of quantified proteins (A) and phosphorylation sites (B). Some clusters of proteins and phosphorylation sites expressed at higher (red) or lower (blue) levels in SCC compared to Pap are highlighted, and a zoom is provided. Heatmap colors represent the median (proteome $n \geq 2$; phosphoproteome $n \geq 3$) of the SILAC ratio.

(C and D) Number of proteins (C) and phosphorylation sites (D) significantly up (Upreg) or downregulated (Downreg) in Pap and SCC compared to TPA. "Only SCC" indicates proteins and phosphorylations sites regulated in SCC but not in Pap.
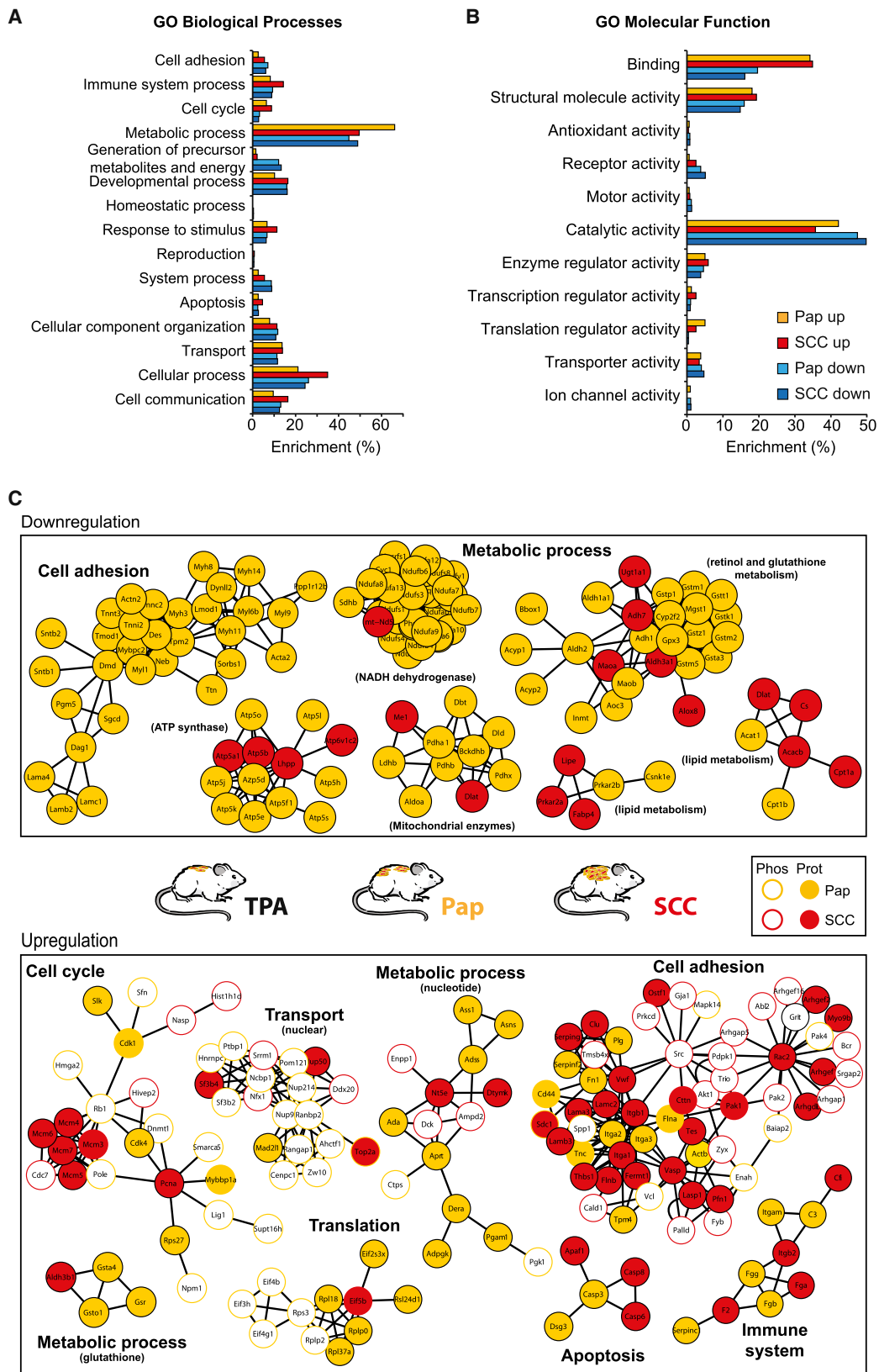
(E) Percentage and number (in brackets) of phosphorylation sites with protein expression level quantified or not.

(F) Comparison between protein expression and phosphorylation levels for the 45% phosphorylation sites in (E). Proteins and phosphorylation sites were considered regulated according to ANOVA test.

See also Tables S4 and S5.

(Figure S3C) and therefore used to extract the cell adhesion subnetwork (Figure 4C). Strikingly, with the exception of Fn1, all of them, as well as most of their first neighbors, were significantly regulated only in the SCC stage. A detailed investigation of the protein identity of this highly connected adhesion subnetwork unveiled proteins tightly associated to the actin

(legend on next page)

cytoskeleton, for example, Vcl, Vasp, Lasp1, Tes, Lima1, and the kinases Src, Pak1, Pak2, and Pak4. Confirming these results, immunofluorescence staining for Vasp and Lima1 on mouse tissues gave stronger staining in SCC compared to Pap and TPA (Figure 5A). Likewise, we observed more intense staining for VASP and LIMA1 in human SCC compared to skin and AK (Figure 5B). Interestingly, Pak4 showed increased phosphorylation levels of the phosphorylation site Ser[181], which we have previously identified in melanoma tissue samples (Zanivan et al., 2008). Ser[181] is located within the linker region of Pak4, suggesting a regulatory function that might be interesting to explore in the future.

Apart from providing a systems level analysis of tumor development, the combined evidence from significantly altered protein and phosphorylation levels highlights a prominent role of cell adhesion mechanisms in the progression of skin carcinoma. Although the concept is not novel (Yu et al., 2011), we identify here a specific subset of highly connected adhesion proteins that potentially contribute to tumor malignancy.

Similarity between Proteomic Changes in Mouse and Gene Expression in Human SCC

Gene expression changes at the mRNA level have been previously measured in two independent studies where normal skin (n = 6) was compared to cutaneous SCC (n = 5) biopsies (Nindl et al., 2006), and normal skin (n = 4) to SCC (n = 11) tissue samples from patients (Riker et al., 2008). We analyzed the concordance of message level changes in human SCC compared to normal skin and the mouse proteomic changes in SCC compared to TPA. We matched the significant mRNA changes against the corresponding protein changes (Table S9), and Figures 5C and 5D show a positive correlation between the two analyses. As specific examples, GPDL1 and ACACB were downregulated at the protein and gene expression levels, in both microarray data sets, while, the intermediate filament KRT16 and the actin-binding protein fascin (FSCN1) were upregulated. Interestingly, FSCN1 has been shown to be involved in several types of SCC (Alam et al., 2012), but not yet skin SCC. Immunofluorescence on mouse and human tissues confirmed high levels of FSCN1 in SCC (Figures 5E–5H).

These results show significant molecular similarities between cutaneous SCC in human patients and in the mouse model used in our study and corroborate the relevance of our proteomic study to provide hints in skin cancer progression in humans.

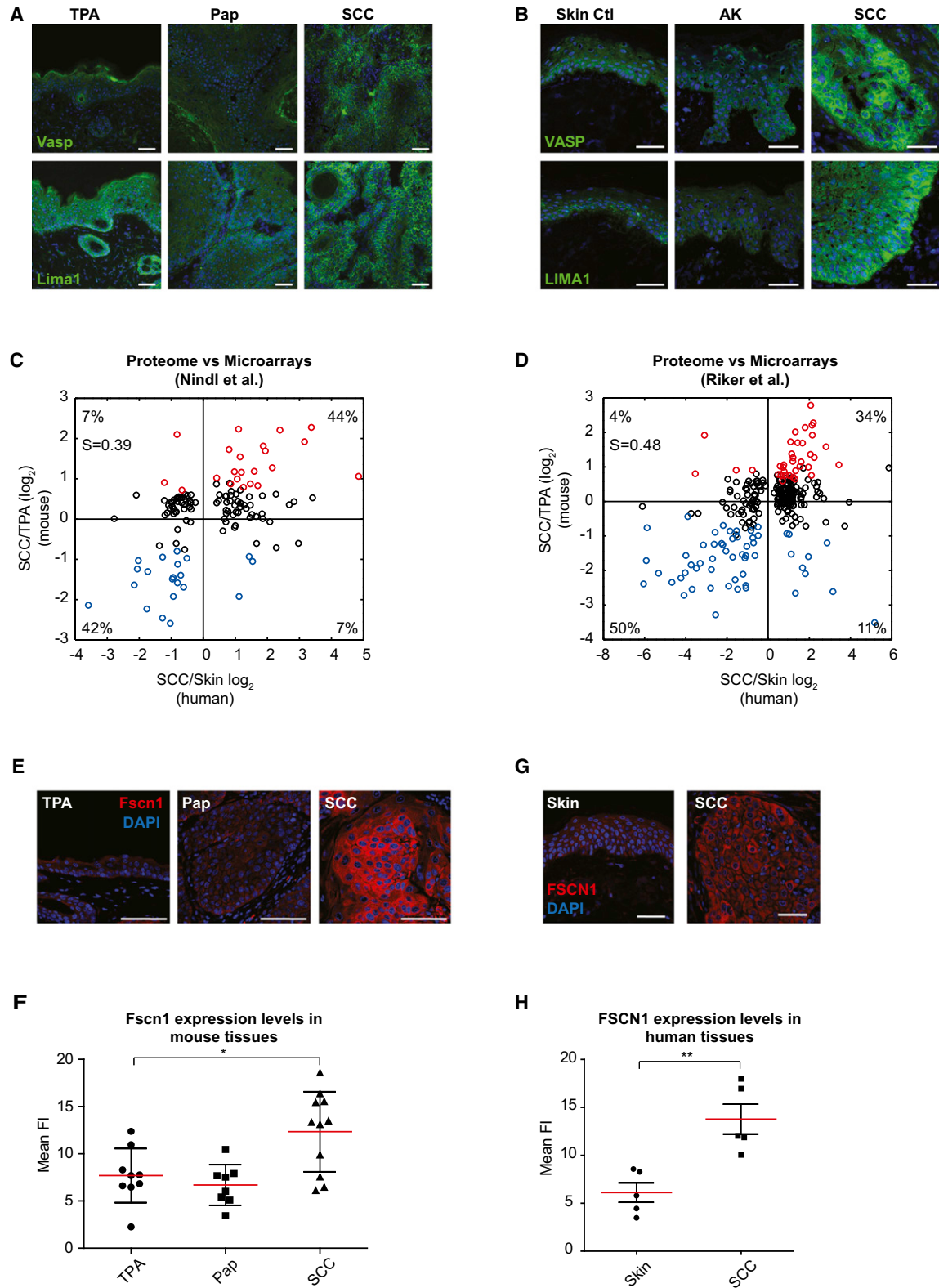### Predicted Kinase Activities in Skin Carcinogenesis

Phosphoproteomic data are a unique resource to determine kinase activity in biological samples, and we interrogated the 825 and 720 phosphorylation sites upregulated in Pap and SCC, respectively, to identify potential deregulated kinases during skin carcinogenesis. By using Motif-X (Schwartz and Gygi, 2005), we identified 13 linear kinase motifs significantly enriched in the Pap and 12 in the SCC. Proline-directed phosphorylations were the major regulated class in both tumors. Also motifs containing acidic amino acids were common to Pap and SCC. Conversely, some motifs were stage specific, such as an additional acidic motif in Pap and motifs containing arginine and lysine in SCC (Figure 6A). To predict the kinases responsible for the phosphorylation of these motifs, we used a prepublication version of the NetworKIN algorithm, where we included the analysis of the 163 kinases identified in our phosphoproteomic study (Jørgensen et al., 2009). Of those, 29 were inferred with significant activity (Figure 6B). For comparison, we included the predicted substrates for a data set containing more than 60,000 observed phosphorylation sites (MegaPhospho). Several proline-directed kinases of the ERK/MAPK, CDK, and GSK3 families and CK2, whose phosphorylation motif contains acidic amino acids, were identified as major tumor-regulated classes. Additionally, as expected, PKC, which is activated upon TPA treatment (DiGiovanni, 1992), was predicted to be highly active in the tumors. Similar predictions were found for PKA and PKD. Interestingly, all of them showed higher predicted activity in SCC compared to Pap, supporting the finding that the arginine-containing motif (PKs motifs may contain an arginine at position −2 or −3) was enriched in SCC but not in Pap (Figure 6A). These results confirmed the patterns observed with Motif-X and pinpointed the likely kinases involved based on cellular context information. Furthermore, the NetworKIN algorithm predicted Pak1, Pak2, and Pak4 to be active in tumors. PAK proteins regulate cell adhesion and are involved in the development of several tumors (Molli et al., 2009), and we investigated them further. The autophosphorylation sites of Pak1 and Pak2, Ser[144] and Ser[141], respectively, which contribute to Pak kinase activation (Chong et al., 2001), increased phosphorylation level during tumor progression (Table S5). In contrast, Ser[181] of Pak4, which is a not yet functionally characterized site, conserved in human, showed similar phosphorylation levels in Pap and SCC, and we investigated PAK4 predicted activity in more detail. Based on observed phosphoproteomic data and kinase activity predictions, we isolated the PAK4 subnetwork (Figure 6C), which unveiled that PAK4 phosphorylates RAF1 (Ser[43]) and SRC (Ser[17]) in SCC but not in Pap. Intriguingly the network predicted that also PKCalpha and PKCdelta phosphorylate SRC (Ser[12]) only in the SCC. While phosphorylation of RAF1 at Ser[43] has been suggested as feedback phosphorylation that negatively regulate RAF1 (Dougherty et al., 2005), phosphorylation at Ser[17] and Ser[12] activate SRC tyrosine kinase activity (Gould and Hunter, 1988). All together, these observations support that SRC activity is increased in skin SCC compared to benign tumor and that this may be triggered by augmented activity of the protein kinases PAK4 and PKC.

Figure 4. Functional and Physical Interaction in Skin Carcinogenesis

(A and B) GO biological processes (A) and molecular functions (B) overrepresented in up- and downregulated proteins in Pap and SCC.

(C) STRING subnetworks of proteins and phosphorylated proteins down (downregulation) and upregulated (upregulation) in SCC. For downregulation, apart for the cell adhesion subnetwork, all the others are related to metabolic processes indicated in brackets. The node color represents regulation at the protein expression level (Prot), while the node border color represents the regulation at the phosphorylation level (Phos) in the Pap and SCC stages.

See also Tables S7, S8, and Figure S3.

Figure 5. Comparison Human Microarrays with Mouse Proteome

(A and B) Confocal images of mouse (A) and human (B) tissue sections stained for LIMA1 and VASP. Nuclei are stained with DAPI (blue). AK, actinic keratosis. Scale bar, 50 μm.

Invasive Role of Phosphoproteins Regulated in Skin Carcinogenesis

To explore the functional relevance of our phosphoproteomic study, we performed invasion assays using the human carcinoma cell lines A431 and SCC9. We chose three cell adhesion proteins for validation: VASP and FSCN1 as they are upregulated in skin SCC (Figure 5), and PAK4, as it is predicted to promote SRC activity in skin SCC. Cells were efficiently silenced for FSCN1, VASP, and PAK4 (Figure S4) and their invasiveness was assessed in a 3D collagen-based invasion assay and a 3D organotypic invasion assay. Strikingly, the silencing of FSCN1, VASP, or PAK4 significantly reduced invasion of A431 (Figures 7A and 7B) and SCC9 (Figures 7C and 7D) compared to cells silenced with the nontargeting small interfering RNA (siRNA) (Figures 7 and S4), indicating that these proteins are part of the invasive machinery of SCC cells.

These results show the functional relevance of our proteomic study in unraveling the proteins, which regulate tumor cell invasion, and that further exploration of our data set might identify potential drug targets for therapies.

DISCUSSION

Here, we have investigated proteome changes in defined stages of skin cancer development. Following upon previous large-scale studies of tumor development at the level of the genome and the transcriptome, the expression levels and phosphorylation status of thousands of proteins have now been accurately quantified throughout cancer progression in a challenging in vivo system. Apart from the SILAC mouse technology, this was made possible by enormous improvements in all aspects of the high-resolution quantitative proteomics pipeline over the last few years. Many protein and phosphorylation changes contained in our data set have already been described in the literature, and thus provide an excellent validation of our screen. These additional regulated protein and phosphorylation changes represent a valuable resource for the cancer research community. Systems-level analysis of our phosphoproteomic data clearly showed that the depth of coverage and quantitative accuracy were sufficient to generate a functional portrait and infer kinase activities of the carcinogenesis process.

The accurate quantification of the proteome of the skin and tumor tissues highlighted major differences in protein expression levels. This may be partly due to the diverse composition of the tissues, such as a higher proportion of dermis in the skin, as suggested by collagen I and skeletal muscle proteins expression levels (Table S3). Such differences were not found between Pap and SCC and therefore were irrelevant for the comparison between tumors. Additionally, the higher expression levels of the integrin heterodimer αmβ2, fibrinogen, and several complement components suggested the presence of inflammatory and blood cells in the tumor tissue. Nevertheless, our proteomic analysis identified clear and distinct differences in protein expression levels between normal keratinocytes and tumor cells (Figures 2 and 5), validating the suitability of our data sets for unveiling molecular mechanisms associated with skin carcinogenesis.

Deregulated Processes in Skin Carcinogenesis

Dedifferentiation is a key feature of cancer development, often used to classify tumors. In our study, we found several components of desmosomes, which are multiprotein complexes that maintain tissue integrity and cell-cell adherence in epithelial tissue, with altered expression levels at the stage of malignancy. By extension, other proteins in our data set that are downregulated specifically in the SCC stage may be novel markers of dedifferentiation and cancer progression.

A key characteristic of cancer is deregulated cell growth and our data revealed broad upregulation of the protein translation machinery already at the Pap stage. Instead, increased phosphorylation levels were associated with regulators of translation and gene expression. Interestingly, the Mcm 2-7 complex, involved in DNA replication initiation and elongation during cell cycle, was highly expressed only in the SCC, indicating further deregulation in malignancy. Metabolism was another major regulated cellular function and changes were already characteristic in benign tumors. In particular, our proteomic data recapitulate the well-known metabolic shift to anaerobic glycolysis, also known as the Warburg effect (Ohlrogge et al., 2009), which we found with different levels of regulation in cancer. For instance, we found upregulation of Pkm2 expression level but downregulation of a specific phosphorylation site. Additionally, we observed changes in the retinol metabolism pathway. Retinol has been shown to be crucial in regulating cell differentiation and induction of antiproliferative genes and retinoid therapy has proven successful to suppress tumor formation in the two stage skin cancer mouse model and several solid tumors in human (Cheepala et al., 2009; Njar et al., 2006). Changes in the redox capacity of cancer cells are well known, and we found that proteins involved in glutathione metabolism changed expression levels already in the Pap.
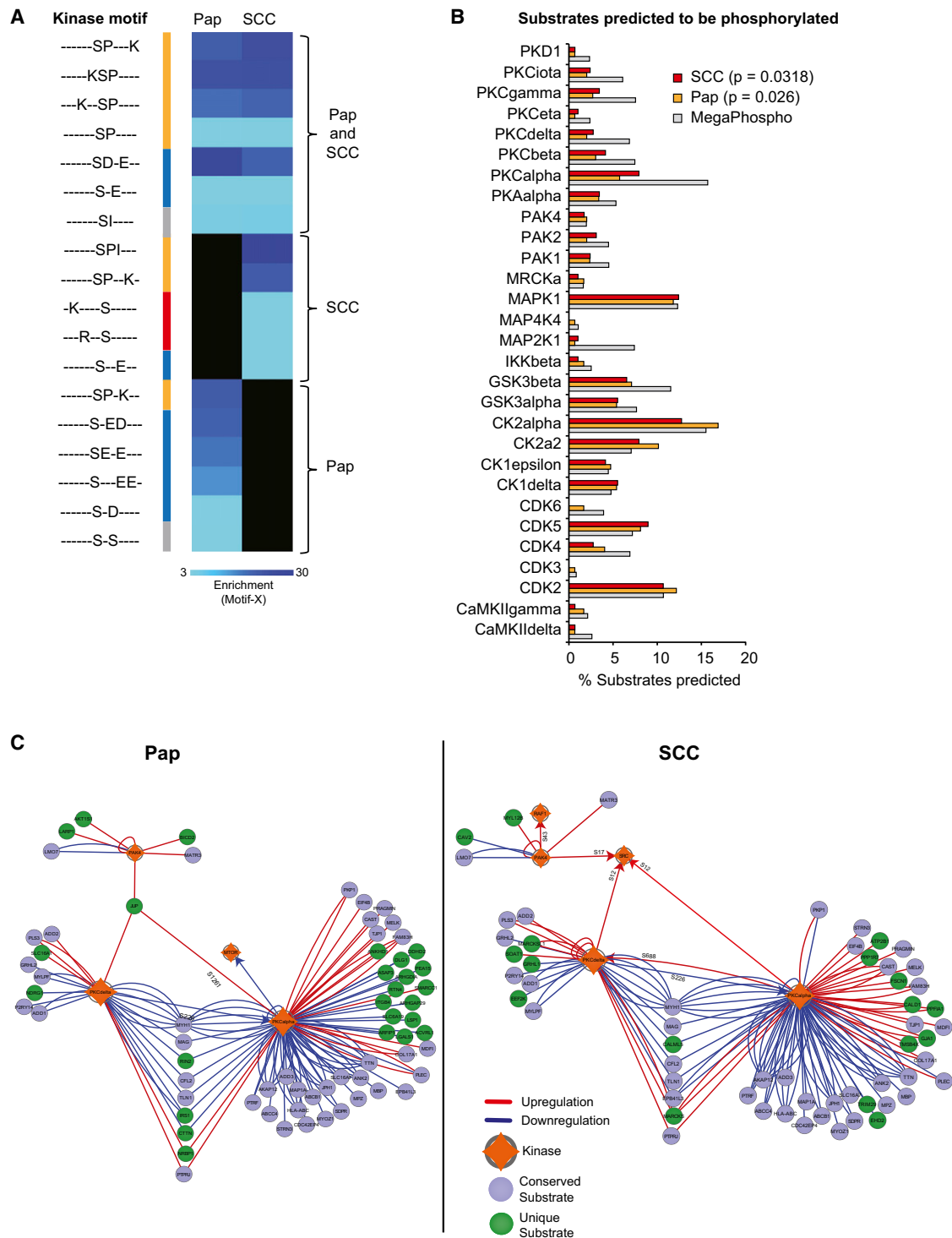
The BM surrounding the tumor cells is remodeled during tumor progression, and BM components can drive tumor malignancy. Laminin 332 is the major BM component expressed in SCC where it regulates cancer cell motility, and its expression level correlates with tumor invasion and patient prognosis (Marinkovich, 2007). In our DMBA-TPA skin carcinogenesis model, laminin 332 had increased expression levels and aberrant deposition in SCC compared to TPA and Pap (Figure 1). Likewise, the major laminin 332 receptor integrin β1 was upregulated specifically in SCC as most of the proteins of the cell adhesion subnetwork. Intriguingly, most of these proteins, including Fscn1, are

---

(C and D) From two independent microarray studies, Nindl et al. (2006) (C) and Riker et al. (2008) (D), the ratios of mRNAs significantly regulated in SCC compared to normal skin in patients are plotted against the ratio calculated in our proteomic study. The percentage in each quadrant indicates the fraction of mRNA significantly regulated also at the protein level. Red, upregulated in SCC; blue, downregulated in SCC, S, Spearman rank correlation.

(E and G) Confocal images of mouse (E) and human (G) tissue sections stained for FSCN1. Scale bar, 78.3 μm (E) and 50 μm (G).

(F and H) Quantification of (E) and (G).
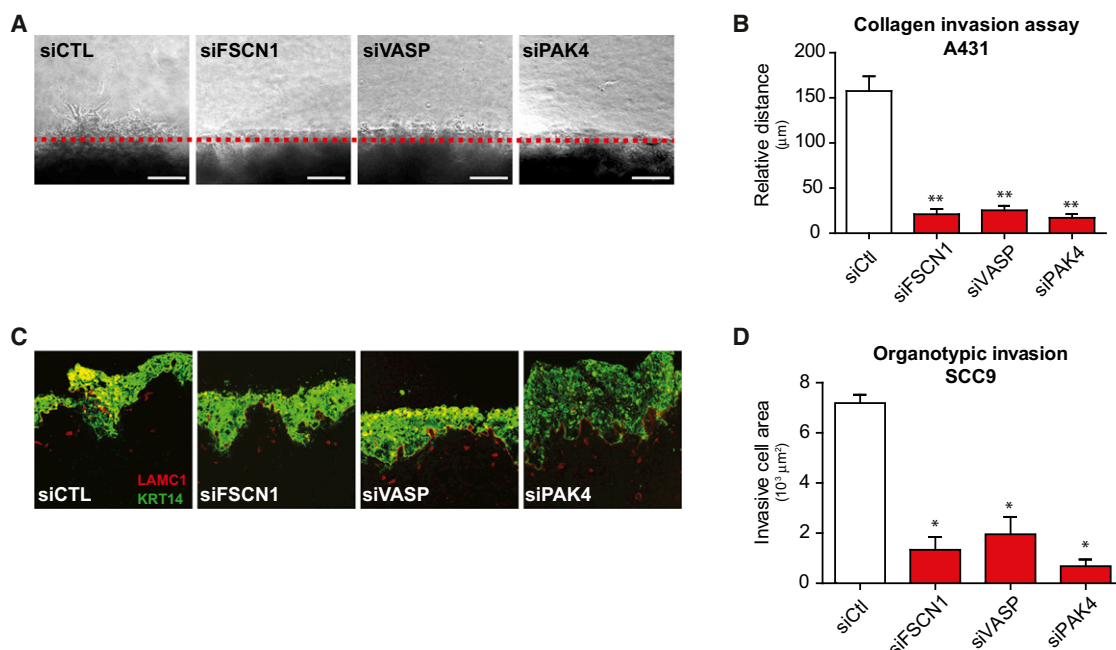
See also Figure S3 and Table S9.

Figure 6. Kinase Activities in Tumors

(A) Heatmap of the linear kinase motifs enriched in Pap and SCC according to Motif-X. Motifs are divided into categories based on the amino acidic composition: proline-directed (yellow), acidic (blue), basic (red), and other (gray).

(B) Kinases predicted to be active in Pap and SCC (p value according to Mann-Whitney Wilcoxon test). On the y axis is represented the percentage of phosphorylated substrates predicted for each kinase.

(C) Extended PAK4 subnetwork, including phosphorylation sites annotation, in Pap and SCC.

Figure 7. Cell Invasion Inhibition by Gene Silencing of FSCN1, VASP, and PAK4

(A) Phase contrast of the invading front of collagen-embedded spheroids composed by A431 cells transfected with nontargeting siRNA (siCTL) or siRNA targeting FSCN1, VASP, and PAK4. The red line indicates where cells start to invade. Error bars = SEM (n = 3). Scale bar, 100μm.

(B) Quantification of (A).

(C) Immunofluorescence of the invading front of SCC9 cells into skin tissue (3D organotypic invasion assay). SCC9 cells were transfected with siCTL or siRNA targeting FSCN1, VASP, and PAK4.

(D) Quantification of (C). Error bars = SEM (n = 3).

p value is according to Mann-Whitney test, single tail. **p = < 0.0001, *p = 0.05. See also Figure S4.

functionally and physically connected to the actin cytoskeleton that is a critical regulator of cancer cell motility and invasion. We provide functional evidence that at least Fscn1, Vasp, and Pak4 can regulate SCC cell invasion. These proteins have previously been shown to regulate tumor cell migration and invasion. It is therefore tempting to speculate that laminin 332, through integrin β1, can activate a specific module of adhesion proteins that regulates the cytoskeletal remodeling needed for cell invasion.

Phosphoproteome Dynamics in Skin Carcinogenesis

Our combined phosphoproteomic data provided a unique opportunity to assess the signaling status of different tumor stages. Because uncontrolled activity of protein kinases is a major tumor-driving cause, we focused our analysis on upregulated phosphorylation sites. Enrichment analysis of substrate motifs together with prediction of kinase activity revealed that specific kinases were associated to the different stages of skin cancer development. MAPK, CDK, and GSK3 activity was common to Pap and SCC, CK1/2 was higher in Pap, whereas PKA, PKC, PKD, and PAK activity was higher in the malignant SCC stage. In depth investigation of the predicted PAK4 and PKC kinase activity discovered that PAK4, PKCalpha, and PKCdelta may promote SRC activity only in SCC. We and others have previously shown that increased Src expression levels in the DMBA-TPA mouse model increases tumor incidence and

burden (Matsumoto et al., 2003; Meves et al., 2011). Our current phosphoproteomic study sheds light on the molecular mechanisms that might be causative to increased SRC activity, whereby PAK4 and PKCs play prominent roles. Furthermore, PAK4 has already been shown to regulate ovarian cancer cell proliferation through a PAK4/SRC/EGFR pathway and that expression levels contribute to poor prognosis in cancer (Siu et al., 2010). We show here that PAK4 regulates SCC cell invasion and our results thus open an exciting perspective to investigate PAK4 in invasion and as a target for anticancer therapies in skin SCC.

In summary, the experimental setup and the mouse model used in this study provides important advantages for the proteomics quantification and interpretation of the results. Applications of the "spike-in" SILAC technology used here (Geiger et al., 2011) should help to extend this approach to other mouse tumor models and human tumors. Moreover, proteomic findings from the mouse model can be verified in human samples using standard techniques (as shown in this study). In particular, it will be interesting to verify the functional importance of the cell adhesion proteins and the PAK4-PKC/SRC subnetwork, which our proteomic data strongly highlighted, in human samples. Likewise, it will be attractive to assess if our findings of specific phosphoproteomic signaling patterns associated with particular stages of tumor development can be generalized to other tumors. Our results clearly imply that it will be fruitful to

interrogate the signaling status of tumors using advanced proteomic technologies.

EXPERIMENTAL PROCEDURES

Tumor Generation and SILAC Mice

Cutaneous two stage chemical carcinogenesis was performed in FVB/N mice as previously described (Roberts et al., 2007). The SILAC mouse colony was generated by fully labeling C57BL/6 mice with $^{13}C_6$ lysine (lysine 6) containing diet (SILANTES) as previously described (Krüger et al., 2008; Zanivan et al., 2012). See also Extended Experimental Procedures.

Mice were housed under the approval and the institutional guidelines governing the care of laboratory mice of the local government of upper Bavaria and in compliance with National and International laws and policies.

Sample Preparation and MS Analysis

Non-TPA-treated and TPA-treated skin, Pap and SCC tumor tissue samples were collected from FVB/N mice of two independent DMBA-TPA experiments. Dissected tissues were homogenized, lysed in 4% SDS, 100 mM DTT, 100 mM Tris HCl lysis buffer. and mixed 1:1 with SILAC skin lysate. For each MS measurement, we pooled tissues collected from 3-6 different mice. Digested peptides were identified on a LTQ-Orbitrap Velos (Thermo Scientific), experiment 1 and 2, or LTQ-Orbitrap Elite (Thermo Scientific), experiment 3. The MS data were processed using the MaxQuant software (Cox and Mann, 2008) and searched with the Andromeda search engine (Cox et al., 2011) against the mouse UniProt database. Only proteins with at least one peptide uniquely assigned to the respective sequence were considered identified. Phosphorylations were assigned as previously described (Olsen et al., 2006). The relative quantification of the peptides and proteins against their SILAC-labeled counterparts was performed by MaxQuant. Quantified proteins (3,457) and phosphorylation sites (5,249) used for the bioinformatic analysis included (1) proteins with a maximum of one missing quantification value within the three MS measurements; (2) phosphorylation sites quantified in at least three MS measurements (Tables S4 and S5). MS RAW data are available on the public repository Tranche. See also Extended Experimental Procedures.

Significantly Regulated Proteins and Phosphorylation Sites

For ANOVA analysis, MS measurements of the same tissues, TPA, Pap, and SCC, were grouped together and the statistical test corrected with permutation based FDR was done with FDR < 0.05 and S0 = 1 as previously described (Tusher et al., 2001). Regulated proteins and phosphorylation sites were considered upregulated or downregulated if the effect size was a positive or negative number, respectively.

Functional and Physical Connections for the Skin Carcinogenesis Portrait

The Uniprot IDs of proteins and phosphorylated proteins regulated in the SCC stage were used to query STRING (Szklarczyk et al., 2011). Two different queries were performed, one for down and one for upregulated proteins. In the latter query, we included actin interactions according to literature data and annotated to the integrin adhesome (Zaidel-Bar and Geiger, 2010), where we assigned to each ITGA and ITGB the specific integrin subunit according to the reference given in the integrin adhesome table (Table S8). The following parameters were used: active prediction methods: experiments, databases, and neighborhood; required confidence (score): high confidence. STRING-determined interactions were visualized in Cytoscape (Cline et al., 2007), and proteins colored according to the stage (Figures S3A and S3B). Cytoscape was also used to generate the connection map where nodes were colored according to the number of edges (Figure S3C). The cell adhesion subnetwork was generated by extracting the nodes with highest number of edges (>12) among the adhesion-related proteins and their first neighbor nodes.

Category Enrichment and Kinase Analysis

GO (Ashburner et al., 2000) analysis has been performed using PantherDB (Mi et al., 2010).

Significantly overrepresented linear kinase motifs were determined by querying the sequence motifs (Table S4) of the phosphorylation sites upregulated in Pap and SCC with Motif-X (Schwartz and Gygi, 2005) against the IPI mouse database, using a p value of E-6 and a minimum number of occurrences of 20.

To predict the kinase activity in the two tumor stages, we used NetworKIN (version 3.0) (see Linding et al., 2007 and R.L. and E.M.S., unpublished data), which can predict substrates for 222 kinases, based on both the linear motifs of the kinase catalytic domain (NetPhorest algorithm [Miller et al., 2008]) and the network context of the kinases. The mouse sequences were matched to the homologous human sequences, and predictions on the up- and downregulated phosphorylation sites in Pap and SCC were generated in the human background. The analysis was performed only on kinases with experimentally identified peptides. The kinase activity enrichment was calculated as ratio between the number of sites predicted by specific kinase and the number of sites identified and quantified in the sample.

To determine significance, the Mann-Whitney Wilcoxon test (p < 0.05) was applied. The MegaPhospho contains 64,232 manually curated phosphorylation sites, integrating (Dinkel et al., 2011) and PhosphositePlus (Hornbeck et al., 2012).

Extended PAK4-centric subnetworks were constructed using the identified and quantified phosphorylation sites in the Pap and SCC samples, for which the regulating kinases were predicted using NetworKIN v3.0. Kinases predicted to interact directly were used in the analysis, including their predicted substrates. A score threshold of 0.1 was applied, and the top 30% of predictions were used. The signaling networks were visualized in Cytoscape.

Microarray Analysis and Comparison with the Proteome

Affymetrix Cel files were normalized and analyzed in Partek Genomics Suite Software, version 6.5. Multiarray Averaging (RMA) method of microarray normalization and summarization was followed by log2 and quantile transformations of the data. Multiway ANOVA was used to identify significantly regulated genes from one of the experimental groups and linear contrasts performed between all pairs of experimental conditions. Multiple test corrections were performed for all calculated p values. Less conservative step up p value was used for further selection of significantly differentially expressed genes.

Chi square and Spearman rank correlation were calculated based on the logarithmized ratio between the median of SCC and skin samples.

Collagen Invasion Assay

3D collagen gel invasion assay was set up as previously described (Lu et al., 2010) with minor modifications (see Extended Experimental Procedures).

3D Organotypic Invasion Assay

The 3D organotypic invasion assays were performed essentially as previously described (Ridky et al., 2010) with modifications (see Extended Experimental Procedures).

Immunofluorescence

Immunostainings have been performed according to standard protocols. Details are reported in the Extended Experimental Procedures.

Statistical Analysis

Unless indicated otherwise, p values have been calculated using a two tail Mann-Whitney test using GraphPad Prism. *p < 0.05; **p < 0.01.

SUPPLEMENTAL INFORMATION

Supplemental Information includes four figures, ten tables, and Extended Experimental Procedures and can be found with this article online at http://dx.doi.org/10.1016/j.celrep.2013.01.003.

REFERENCES

Abel, E.L., Angel, J.M., Kiguchi, K., and DiGiovanni, J. (2009). Multi-stage chemical carcinogenesis in mouse skin: fundamentals and applications. Nat. Protoc. 4, 1350–1362.

Alam, H., Bhate, A.V., Gangadaran, P., Sawant, S.S., Salot, S., Sehgal, L., Dange, P.P., Chaukar, D.A., D'cruz, A.K., Kannanl, S., et al. (2012). Fascin overexpression promotes neoplastic progression in oral squamous cell carcinoma. BMC Cancer 12, 32.

Ashburner, M., Ball, C.A., Blake, J.A., Botstein, D., Butler, H., Cherry, J.M., Davis, A.P., Dolinski, K., Dwight, S.S., Eppig, J.T., et al.; The Gene Ontology Consortium. (2000). Gene ontology: tool for the unification of biology. Nat. Genet. 25, 25–29.

Cheepala, S.B., Yin, W., Syed, Z., Gill, J.N., McMillian, A., Kleiner, H.E., Lynch, M., Loganantharaj, R., Trutschl, M., Cvek, U., and Clifford, J.L. (2009). Identification of the B-Raf/Mek/Erk MAP kinase pathway as a target for all-trans retinoic acid during skin cancer promotion. Mol. Cancer 8, 27.

Chong, C., Tan, L., Lim, L., and Manser, E. (2001). The mechanism of PAK activation. Autophosphorylation events in both regulatory and kinase domains control activity. J. Biol. Chem. 276, 17347–17353.

Cline, M.S., Smoot, M., Cerami, E., Kuchinsky, A., Landys, N., Workman, C., Christmas, R., Avila-Campilo, I., Creech, M., Gross, B., et al. (2007). Integration of biological networks and gene expression data using Cytoscape. Nat. Protoc. 2, 2366–2382.

Cox, J., and Mann, M. (2008). MaxQuant enables high peptide identification rates, individualized p.p.b.-range mass accuracies and proteome-wide protein quantification. Nat. Biotechnol. 26, 1367–1372.

Cox, J., Neuhauser, N., Michalski, A., Scheltema, R.A., Olsen, J.V., and Mann, M. (2011). Andromeda: a peptide search engine integrated into the MaxQuant environment. J. Proteome Res. 10, 1794–1805.

Davies, H., Bignell, G.R., Cox, C., Stephens, P., Edkins, S., Clegg, S., Teague, J., Woffendin, H., Garnett, M.J., Bottomley, W., et al. (2002). Mutations of the BRAF gene in human cancer. Nature 417, 949–954.

DiGiovanni, J. (1992). Multistage carcinogenesis in mouse skin. Pharmacol. Ther. 54, 63–128.

Dinkel, H., Chica, C., Via, A., Gould, C.M., Jensen, L.J., Gibson, T.J., and Diella, F. (2011). Phospho.ELM: a database of phosphorylation sites—update 2011. Nucleic Acids Res. 39(Database issue), D261–D267.

Dougherty, M.K., Müller, J., Ritt, D.A., Zhou, M., Zhou, X.Z., Copeland, T.D., Conrads, T.P., Veenstra, T.D., Lu, K.P., and Morrison, D.K. (2005). Regulation of Raf-1 by direct feedback phosphorylation. Mol. Cell 17, 215–224.

Ehrenreiter, K., Kern, F., Velamoor, V., Meissl, K., Galabova-Kovacs, G., Sibilia, M., and Baccarini, M. (2009). Raf-1 addiction in Ras-induced skin carcinogenesis. Cancer Cell 16, 149–160.

Geiger, T., Wisniewski, J.R., Cox, J., Zanivan, S., Kruger, M., Ishihama, Y., and Mann, M. (2011). Use of stable isotope labeling by amino acids in cell culture as a spike-in standard in quantitative proteomics. Nat. Protoc. 6, 147–157.

Gould, K.L., and Hunter, T. (1988). Platelet-derived growth factor induces multisite phosphorylation of pp60c-src and increases its protein-tyrosine kinase activity. Mol. Cell. Biol. 8, 3345–3356.

Hanahan, D., and Weinberg, R.A. (2011). Hallmarks of cancer: the next generation. Cell 144, 646–674.

Hanash, S., and Taguchi, A. (2010). The grand challenge to decipher the cancer proteome. Nat. Rev. Cancer 10, 652–660.

Harsha, H.C., and Pandey, A. (2010). Phosphoproteomics in cancer. Mol. Oncol. 4, 482–495.

Hornbeck, P.V., Kornhauser, J.M., Tkachev, S., Zhang, B., Skrzypek, E., Murray, B., Latham, V., and Sullivan, M. (2012). PhosphoSitePlus: a comprehensive resource for investigating the structure and function of experimentally determined post-translational modifications in man and mouse. Nucleic Acids Res. 40(Database issue), D261–D270.

Hummerich, L., Müller, R., Hess, J., Kokocinski, F., Hahn, M., Fürstenberger, G., Mauch, C., Lichter, P., and Angel, P. (2006). Identification of novel tumour-associated genes differentially expressed in the process of squamous cell cancer development. Oncogene 25, 111–121.

Jørgensen, C., Sherman, A., Chen, G.I., Pasculescu, A., Poliakov, A., Hsiung, M., Larsen, B., Wilkinson, D.G., Linding, R., and Pawson, T. (2009). Cell-specific information processing in segregating populations of Eph receptor ephrin-expressing cells. Science 326, 1502–1509.

Krüger, M., Moser, M., Ussar, S., Thievessen, I., Luber, C.A., Forner, F., Schmidt, S., Zanivan, S., Fässler, R., and Mann, M. (2008). SILAC mouse for quantitative proteomics uncovers kindlin-3 as an essential factor for red blood cell function. Cell 134, 353–364.

Kurzen, H., Münzing, I., and Hartschuh, W. (2003). Expression of desmosomal proteins in squamous cell carcinomas of the skin. J. Cutan. Pathol. 30, 621–630.

Landis, M.D., Seachrist, D.D., Montañez-Wiscovich, M.E., Danielpour, D., and Keri, R.A. (2005). Gene expression profiling of cancer progression reveals intrinsic regulation of transforming growth factor-beta signaling in ErbB2/Neu-induced tumors from transgenic mice. Oncogene 24, 5173–5190.

Larsen, M.R., Thingholm, T.E., Jensen, O.N., Roepstorff, P., and Jørgensen, T.J. (2005). Highly selective enrichment of phosphorylated peptides from peptide mixtures using titanium dioxide microcolumns. Mol. Cell. Proteomics 4, 873–886.

Linding, R., Jensen, L.J., Ostheimer, G.J., van Vugt, M.A., Jørgensen, C., Miron, I.M., Diella, F., Colwill, K., Taylor, L., Elder, K., et al. (2007). Systematic discovery of in vivo phosphorylation networks. Cell 129, 1415–1426.

Lu, C., Li, X.Y., Hu, Y., Rowe, R.G., and Weiss, S.J. (2010). MT1-MMP controls human mesenchymal stem cell trafficking and differentiation. Blood 115, 221–229.

Mann, M. (2006). Functional and quantitative proteomics using SILAC. Nat. Rev. Mol. Cell Biol. 7, 952–958.

Marcotte, R., and Muller, W.J. (2008). Signal transduction in transgenic mouse models of human breast cancer—implications for human breast cancer. J. Mammary Gland Biol. Neoplasia 13, 323–335.

Marinkovich, M.P. (2007). Tumour microenvironment: laminin 332 in squamous-cell carcinoma. Nat. Rev. Cancer 7, 370–380.

Matsumoto, T., Jiang, J., Kiguchi, K., Ruffino, L., Carbajal, S., Beltrán, L., Bol, D.K., Rosenberg, M.P., and DiGiovanni, J. (2003). Targeted expression of c-Src in epidermal basal cells leads to enhanced skin tumor promotion, malignant progression, and metastasis. Cancer Res. 63, 4819–4828.

Meves, A., Geiger, T., Zanivan, S., DiGiovanni, J., Mann, M., and Fässler, R. (2011). Beta1 integrin cytoplasmic tyrosines promote skin tumorigenesis independent of their phosphorylation. Proc. Natl. Acad. Sci. USA 108, 15213–15218.

Mi, H., Dong, Q., Muruganujan, A., Gaudet, P., Lewis, S., and Thomas, P.D. (2010). PANTHER version 7: improved phylogenetic trees, orthologs and collaboration with the Gene Ontology Consortium. Nucleic Acids Res. 38(Database issue), D204–D210.

Miller, M.L., Jensen, L.J., Diella, F., Jørgensen, C., Tinti, M., Li, L., Hsiung, M., Parker, S.A., Bordeaux, J., Sicheritz-Ponten, T., et al. (2008). Linear motif atlas for phosphorylation-dependent signaling. Sci. Signal. 1, ra2.

Molli, P.R., Li, D.Q., Murray, B.W., Rayala, S.K., and Kumar, R. (2009). PAK signaling in oncogenesis. Oncogene 28, 2545–2555.

Monetti, M., Nagaraj, N., Sharma, K., and Mann, M. (2011). Large-scale phosphosite quantification in tissues by a spike-in SILAC method. Nat. Methods 8, 655–658.

Nilsson, K., Svensson, S., and Landberg, G. (2004). Retinoblastoma protein function and p16INK4a expression in actinic keratosis, squamous cell carcinoma in situ and invasive squamous cell carcinoma of the skin and links between p16INK4a expression and infiltrative behavior. Mod. Pathol. 17, 1464–1474.

Nindl, I., Dang, C., Forschner, T., Kuban, R.J., Meyer, T., Sterry, W., and Stockfleth, E. (2006). Identification of differentially expressed genes in cutaneous squamous cell carcinoma by microarray expression profiling. Mol. Cancer 5, 30.

Njar, V.C., Gediya, L., Purushottamachar, P., Chopra, P., Vasaitis, T.S., Khandelwal, A., Mehta, J., Huynh, C., Belosay, A., and Patel, J. (2006). Retinoic acid metabolism blocking agents (RAMBAs) for treatment of cancer and dermatological diseases. Bioorg. Med. Chem. 14, 4323–4340.

Ohlrogge, J., Allen, D., Berguson, B., Dellapenna, D., Shachar-Hill, Y., and Stymne, S. (2009). Energy. Driving on biomass. Science 324, 1019–1020.

Olsen, J.V., Blagoev, B., Gnad, F., Macek, B., Kumar, C., Mortensen, P., and Mann, M. (2006). Global, in vivo, and site-specific phosphorylation dynamics in signaling networks. Cell 127, 635–648.

Ong, S.E., Blagoev, B., Kratchmarova, I., Kristensen, D.B., Steen, H., Pandey, A., and Mann, M. (2002). Stable isotope labeling by amino acids in cell culture, SILAC, as a simple and accurate approach to expression proteomics. Mol. Cell. Proteomics 1, 376–386.

Ostasiewicz, P., Zielinska, D.F., Mann, M., and Wiśniewski, J.R. (2010). Proteome, phosphoproteome, and N-glycoproteome are quantitatively preserved in formalin-fixed paraffin-embedded tissue and analyzable by high-resolution mass spectrometry. J. Proteome Res. 9, 3688–3700.

Pawson, T., and Scott, J.D. (2005). Protein phosphorylation in signaling—50 years and counting. Trends Biochem. Sci. 30, 286–290.

Reddy, E.P., Reynolds, R.K., Santos, E., and Barbacid, M. (1982). A point mutation is responsible for the acquisition of transforming properties by the T24 human bladder carcinoma oncogene. Nature 300, 149–152.

Ridky, T.W., Chow, J.M., Wong, D.J., and Khavari, P.A. (2010). Invasive three-dimensional organotypic neoplasia from multiple normal human epithelia. Nat. Med. 16, 1450–1455.

Riker, A.I., Enkemann, S.A., Fodstad, O., Liu, S., Ren, S., Morris, C., Xi, Y., Howell, P., Metge, B., Samant, R.S., et al. (2008). The gene expression profiles of primary and metastatic melanoma yields a transition point of tumor progression and metastasis. BMC Med. Genomics 1, 13.

Rikova, K., Guo, A., Zeng, Q., Possemato, A., Yu, J., Haack, H., Nardone, J., Lee, K., Reeves, C., Li, Y., et al. (2007). Global survey of phosphotyrosine signaling identifies oncogenic kinases in lung cancer. Cell 131, 1190–1203.

Ritt, D.A., Monson, D.M., Specht, S.I., and Morrison, D.K. (2010). Impact of feedback phosphorylation and Raf heterodimerization on normal and mutant B-Raf signaling. Mol. Cell. Biol. 30, 806–819.

Roberts, S.J., Ng, B.Y., Filler, R.B., Lewis, J., Glusac, E.J., Hayday, A.C., Tigelaar, R.E., and Girardi, M. (2007). Characterizing tumor-promoting T cells in chemically induced cutaneous carcinogenesis. Proc. Natl. Acad. Sci. USA 104, 6770–6775.

Roesch, A., Becker, B., Meyer, S., Hafner, C., Wild, P.J., Landthaler, M., and Vogt, T. (2005). Overexpression and hyperphosphorylation of retinoblastoma protein in the progression of malignant melanoma. Mod. Pathol. 18, 565–572.

Schwartz, D., and Gygi, S.P. (2005). An iterative statistical approach to the identification of protein phosphorylation motifs from large-scale data sets. Nat. Biotechnol. 23, 1391–1398.

Siu, M.K., Chan, H.Y., Kong, D.S., Wong, E.S., Wong, O.G., Ngan, H.Y., Tam, K.F., Zhang, H., Li, Z., Chan, Q.K., et al. (2010). p21-activated kinase 4 regulates ovarian cancer cell proliferation, migration, and invasion and contributes to poor prognosis in patients. Proc. Natl. Acad. Sci. USA 107, 18622–18627.

Stratton, M.R., Campbell, P.J., and Futreal, P.A. (2009). The cancer genome. Nature 458, 719–724.

Szklarczyk, D., Franceschini, A., Kuhn, M., Simonovic, M., Roth, A., Minguez, P., Doerks, T., Stark, M., Muller, J., Bork, P., et al. (2011). The STRING database in 2011: functional interaction networks of proteins, globally integrated and scored. Nucleic Acids Res. 39(Database issue), D561–D568.

Tian, Q., Stepaniants, S.B., Mao, M., Weng, L., Feetham, M.C., Doyle, M.J., Yi, E.C., Dai, H., Thorsson, V., Eng, J., et al. (2004). Integrated genomic and proteomic analyses of gene expression in Mammalian cells. Mol. Cell. Proteomics 3, 960–969.

Tusher, V.G., Tibshirani, R., and Chu, G. (2001). Significance analysis of microarrays applied to the ionizing radiation response. Proc. Natl. Acad. Sci. USA 98, 5116–5121.

Villén, J., Beausoleil, S.A., Gerber, S.A., and Gygi, S.P. (2007). Large-scale phosphorylation analysis of mouse liver. Proc. Natl. Acad. Sci. USA 104, 1488–1493.

Walrath, J.C., Hawes, J.J., Van Dyke, T., and Reilly, K.M. (2010). Genetically engineered mouse models in cancer research. Adv. Cancer Res. 106, 113–164.

Wang, L., Harris, T.E., and Lawrence, J.C., Jr. (2008). Regulation of proline-rich Akt substrate of 40 kDa (PRAS40) function by mammalian target of rapamycin complex 1 (mTORC1)-mediated phosphorylation. J. Biol. Chem. 283, 15619–15627.

Wisniewski, J.R., Zougman, A., Nagaraj, N., and Mann, M. (2009). Universal sample preparation method for proteome analysis. Nat. Methods 6, 359–362.

Wong, M.P., Cheang, M., Yorida, E., Coldman, A., Gilks, C.B., Huntsman, D., and Berean, K. (2008). Loss of desmoglein 1 expression associated with worse prognosis in head and neck squamous cell carcinoma patients. Pathology 40, 611–616.

Yu, H., Mouw, J.K., and Weaver, V.M. (2011). Forcing form and function: biomechanical regulation of tumor evolution. Trends Cell Biol. 21, 47–56.

Zaidel-Bar, R., and Geiger, B. (2010). The switchable integrin adhesome. J. Cell Sci. 123, 1385–1388.

Zanivan, S., Gnad, F., Wickström, S.A., Geiger, T., Macek, B., Cox, J., Fässler, R., and Mann, M. (2008). Solid tumor proteome and phosphoproteome analysis by high resolution mass spectrometry. J. Proteome Res. 7, 5314–5326.

Zanivan, S., Krueger, M., and Mann, M. (2012). In vivo quantitative proteomics: the SILAC mouse. Methods Mol. Biol. 757, 435–450.